

Measurement of the ground-state flux diagram of three coupled qubits as a first step towards the demonstration of adiabatic quantum computation

A. IZMALKOV¹(*), M. GRAJCAR², S. H. W. VAN DER PLOEG¹, U. HÜBNER¹, E. IL'ICHEV¹(**), H.-G. MEYER¹ and A. M. ZAGOSKIN³

¹ *Institute for Physical High Technology, P.O. Box 100239, D-07702 Jena, Germany*

² *Department of Solid State Physics, Comenius University,
SK-84248 Bratislava, Slovakia*

³ *Physics and Astronomy Dept., The University of British Columbia,
6224 Agricultural Rd., Vancouver, B.C., V6T 1Z1 Canada*

PACS. 85.25.Cp – Josephson devices.

PACS. 85.25.Dq – SQUIDs.

PACS. 03.67.Lx – Quantum computation.

Abstract. – The ground state susceptibility of a system consisting of three flux-qubits was measured in the complete three dimensional flux space around the common degeneracy point of the qubits. The system's Hamiltonian could be completely reconstructed from measurements made far away from the common degeneracy point. The subsequent measurements made around this point show complete agreement with the theoretical predictions which follow from this Hamiltonian. The ground state anti-crossings of the system could be read-out directly from these measurements. This allows one to determine the ground-state flux diagram, which provides the solution for the non-polynomial optimization problem MAXCUT encoded in the Hamiltonian of the three-flux-qubit system. Our results show that adiabatic quantum computation can be demonstrated with this system provided that the energy gap and/or the speed of the read-out is increased.

In the field of solid state qubits superconducting Josephson junctions qubits are one of the most promising candidates for quantum computation [1]. Currently they are attracting considerable attention, mostly, because they are potentially scalable, can be accessed relatively easily and controlled individually. Quantum coherent oscillations and conditional gate operation have been demonstrated in a two-qubit system [2–4], entanglement between the qubit and detector was achieved recently [5, 6], and a lot of attempts have been made in the direction of improvement the qubit's coherent dynamic [7]. These experiments were aimed to construct a universal set of gates as a basis for quantum computation.

An alternative approach is adiabatic quantum computation (AQC) [8]. It is based on the encoding of a non-polynomially hard problem in a complex multi-qubit Hamiltonian. This

(*) E-mail: andrei.izmalkov@ipht-jena.de

(**) E-mail: ilichev@ipht-jena.de

encoding should be done in such a way that the ground state gives the solution of the problem. In order to reach this ground state adiabatic quantum evolution of the systems Hamiltonian is used. As a preparation step, the system is moved to a flux configuration where it can easily relax to the ground state. In the subsequent calculation step, the system adiabatically evolves to the configuration where its ground state encodes a non-polynomial hard problem. In the final step, this ground state should be readout. A scalable architecture for AQC using superconducting qubits was proposed by Kaminsky *et al.* [9] and the equivalence of AQC to standard quantum computation has been shown by Aharonov *et al.* [10].

For flux qubits, such a controllable Hamiltonian can be built up by making use of the flux dependence of their energies. Therefore, the (energy) eigenvalues of this Hamiltonian become a N -dimensional function of the flux through each qubit: $E_i(f_{q1}, f_{q2}, \dots, f_{qN})$ with $f_{qi} = \Phi_{qi}/\Phi_0 - 0.5$ being the flux normalized by the flux quantum $\Phi_0 = \hbar/2e$ relative to the degeneracy point of the qubit. The eigenstates of this Hamiltonian can be described as a superposition of the 2^N states in the natural qubit ($|\downarrow\rangle$ or $|\uparrow\rangle$) basis: $\Psi = \alpha_1|\downarrow_1\downarrow_2 \dots \downarrow_N\rangle + \alpha_2|\uparrow_1\downarrow_2 \dots \downarrow_N\rangle + \dots + \alpha_{2^N}|\uparrow_1\uparrow_2 \dots \uparrow_N\rangle$. If we set the fluxes far away from the degeneracy point of each qubit, i.e. $|f_{qi}| \gg 0$, then the system is neither entangled nor in a superposition of states but just in the simple classical state: $\alpha_j = 1$, $\alpha_1 = \dots = \alpha_{j-1} = \alpha_{j+1} = \dots = \alpha_{2^N} = 0$. If the fluxes through all coupled qubits are close to their degeneracies, then we approach the *common* degeneracy point of the whole system, where its state is maximally entangled. Close to this degeneracy point the N -dimensional energy surface has a rich structure with significant curvature. From this curvature, which is directly proportional to the system's susceptibility, the qubits' state can be determined [14]. In this Letter we show the complete characterization of the susceptibility of a three flux qubit system around its common degeneracy point.

The susceptibility can be determined by using a radio-frequency tank circuit. In this technique the tank circuit plays the role of a parametric transducer, since any variation of the real part susceptibility χ of, for instance, the superconducting interferometers [12, 13] is transformed to a change of the tank's resonance frequency. The variation of the resonance frequency can be detected by measuring the phase shift θ between the *ac*-current I_{rf} applied through the coil and *ac*-voltage over the tank circuit. These quantities are related through

$$\tan \theta = -\frac{Q_{\text{T}}}{L_{\text{T}}} \chi, \quad (1)$$

where L_{T} is the tank coil inductance and Q_{T} its quality.

For a multi-qubit system in the ground state $\chi = -M_{q\text{T}}^2 \frac{d^2 E_0}{(d\Phi_{b\text{T}})^2}$, where E_0 is the qubit's ground state energy, $M_{q\text{T}}$ is the qubit-tank mutual inductance and $\Phi_{b\text{T}}$ is the external flux applied to the qubits by the coil. The band curvature is maximal near the anti-crossings of the energy levels. These anti-crossings are located close to the degeneracies of the classical states ($\Delta_i = 0$), e.g. $E(\uparrow\uparrow\downarrow) = E(\downarrow\uparrow\downarrow)$ for three qubits. Therefore this method allows one to find the location of classical crossings in the full flux space of a multi qubit system. For finite temperatures, in addition, the higher states become populated thereby allowing the readout of their anti-crossings [15].

The effective Hamiltonian for three coupled qubits is

$$H = -\sum_{i=1}^3 [\epsilon_i \sigma_z^{(i)} + \Delta_i \sigma_x^{(i)}] + \sum_{1 \leq i < j \leq 3} J_{ij} \sigma_z^{(i)} \sigma_z^{(j)}, \quad (2)$$

with ϵ_i the energy bias on qubit i , Δ_i its tunnelling amplitude, J_{ij} the coupling energy between qubits i and j , and σ_z , σ_x are the Pauli matrices in the natural basis of $|\downarrow\rangle$ ($\langle\downarrow|\sigma_z|\downarrow\rangle = -1$) and

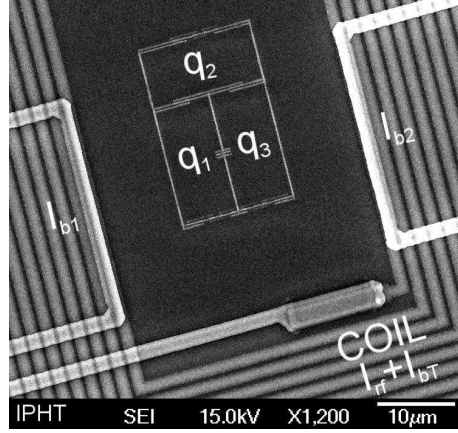


Fig. 1 – Electron micrograph of the sample. The qubits are coupled by $120 \times 2000 \text{ nm}^2$ shared Josephson junctions. Each loop also contains three Josephson junctions forming the qubit. Two of these are $120 \times 600 \text{ nm}^2$ while a third one is 35% smaller. Qubits are fabricated inside an LC resonator coil, which is part of the resonant circuit performing the readout of the qubit *ac*-susceptibility. The flux through the qubits can be individually controlled by *dc*-currents through the coil I_{bT} , and two additional lines I_{b1} and I_{b2} .

$|\uparrow\rangle$ ($\langle\uparrow|\sigma_z|\uparrow\rangle = 1$). Depending on the sign of J_{ij} such a Hamiltonian can describe systems with anti-ferromagnetic [18, 19] and ferro-magnetic [20] interactions as well as a system with both types of interaction [17]. The sample described here has only anti-ferromagnetic interactions. As a result the system becomes frustrated around its common degeneracy point. In fact, in the classical limit ($\Delta_i \rightarrow 0$) the Hamiltonian (2) encodes the non-polynomial MAXCUT problem [14, 16]. The solution of this optimization problem is the classical state with the lowest energy. By using the adiabatic evolution of the quantum system (2) with $\Delta_i \neq 0$ one can find all anti-crossings of the ground state and reconstruct the classical cross-overs from them. As was explained in Ref. [14], this information allows one to determine the classical state which corresponds to the solution of MAXCUT problem ⁽¹⁾.

Figure 1 shows the sample measured which consists of three Al persistent current qubits [11] placed inside a Nb pancake coil. The areas of the Al loops are $14 \times 7 \mu\text{m}^2$. Two junctions in each qubit are nominally $600 \times 120 \text{ nm}^2$, while a third one is $\sim 35\%$ smaller. The qubits are coupled to each other both magnetically and via shared junctions [15, 21]. Each coupling junction has approximately the same area of $120 \times 2000 \text{ nm}^2$. The flux through the qubits can be individually controlled by *dc* currents through the coil I_{bT} , and two additional lines I_{b1} and I_{b2} . The Nb coil has an inductance $L_T = 134 \text{ nH}$, and together with an external capacitance $C_T = 470 \text{ pF}$ forms a parallel tank circuit with $\omega_T/2\pi = 20.038 \text{ MHz}$ and quality $Q_T = \omega_T R_T C_T = 700$ (here R_T is the effective resistance). The qubits were fabricated by *e*-beam lithography and two-angle shadow evaporation, whereas the Nb coil was made by *e*-beam lithography and CF_4 reactive-ion etching.

The qubit-coil mutual inductances were extracted from the Φ_0 periodicity of the *ac*-susceptibility of the individual qubit as $M_{q1,T} \approx 45.77 \text{ pH}$ and $M_{q2,T} \approx 46.62 \text{ pH}$, $M_{q3,T} \approx 45.79 \text{ pH}$. Fig 2 plots the tangent of the phase shift $-\tan\theta(I_{bT}, I_{bj})$ ($j = 1, 2$), as measured at the mixing chamber temperature of 10 mK. The Hamiltonian itself was completely

⁽¹⁾as an example, for the present system with $f_{q1} = 0.008$, $f_{q2} = 0.02$ and $f_{q3} = 0$ the solution of MAXCUT problem is described by the state $|\uparrow\uparrow\downarrow\rangle$, see Fig. 3b

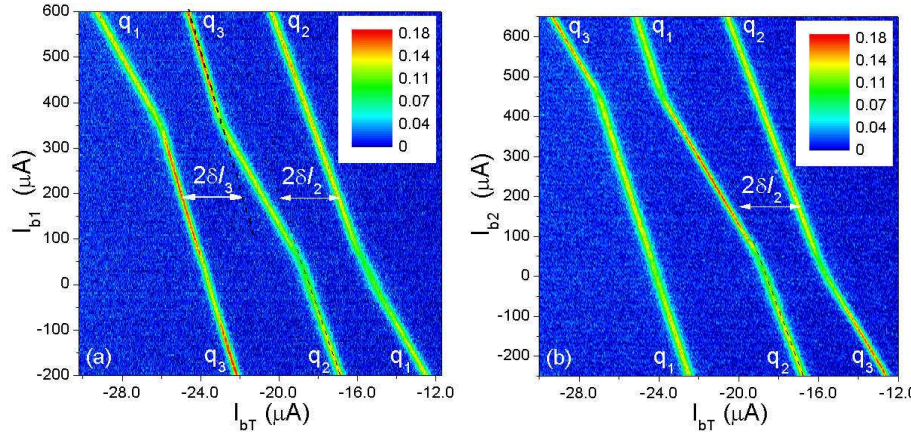


Fig. 2 – (a) – $-\tan \theta(I_{bT}, I_{b1})$ at $I_{b2} = 400 \mu\text{A}$. The qubits' coupling strength $J_{12}/I_{p2}\Phi_0 = M_{q2T}\delta I_2/\Phi_0 \approx 0.034$ and $J_{13}/I_{p3}\Phi_0 = M_{q3T}\delta I_3/\Phi_0 \approx 0.033$. (b) – $-\tan \theta(I_{bT}, I_{b2})$ at $I_{b1} = -400 \mu\text{A}$. The coupling strength between qubits 2 and 3 is $J_{23}/I_{p2}\Phi_0 = M_{q2T}\delta I_2^*/\Phi_0 \approx 0.034$. The repulsion between the traces (q_1, q_2) , (q_1, q_3) and (q_2, q_3) confirms the anti-ferromagnetic coupling between the qubits in these pairs.

reconstructed from a number of scans away from the common degeneracy point. Each trace corresponds to a single qubit anti-crossing, while the repulsion between them confirms the *anti-ferromagnetic* coupling between all pairs of qubits [15]. The individual qubit parameters (persistent currents I_{pi} and tunnelling amplitudes Δ_i) were found from the shape of the peaks, $-\tan \theta(f_{bT})$, when all other qubits were biased away from their degeneracy [22] (as an example we can choose the curve $-\tan \theta(f_{bT})$ for $I_{b1} = 600 \mu\text{A}$ and $I_{b2} = 400 \mu\text{A}$). The coupling amplitude J_{ij} between all pairs of qubits can be obtained by measuring the peak-to-peak distance $\delta f_i = M_{qiT}\delta I_i/\Phi_0$ [15], see Fig 2. Thus, the dimensionless coupling energy is equal to δf_i , i.e. $J_{ij}/I_{pi}\Phi_0 = \delta f_i$. The reconstruction of the parameters resulted in $\Delta_1 \approx \Delta_2 \approx \Delta_3 = 70 \text{ mK}$, $I_{p1} \approx I_{p2} = 115 \text{ nA}$, $I_{p3} = 125 \text{ nA}$, $J_{12}/I_{p2}\Phi_0 = M_{q2T}\delta I_2/\Phi_0 = 0.034$, $J_{13}/I_{p3}\Phi_0 = M_{q3T}\delta I_3/\Phi_0 = 0.033$ and $J_{23}/I_{p2}\Phi_0 = M_{q2T}\delta I_2^*/\Phi_0 = 0.034$, at the effective temperature $T_{\text{eff}} = 70 \text{ mK}$ of our setup known from previous experiments [15, 17]. The discrepancy between effective and mixing-chamber temperature is due to the noise from external leads and amplifier back-action. The substitution of the persistent currents into the later three expressions gives $J_{12} \approx J_{13} \approx J_{23} = (0.61 \pm 0.02) \text{ K}$. The slope of the traces in Fig 2 gives the mutual inductances between qubits and *dc*-bias lines. We found $M_{q1,b1} = 0.595$, $M_{q2,b1} = 0.387$, $M_{q3,b1} = 0.329$, $M_{q1,b2} = 0.296$ and $M_{q2,b2} = 0.347$, $M_{q3,b2} = 0.543$ (all in pH).

The experimental reconstruction of the mutual inductance matrix $M_{qi,bi}$ ($bi = b1, b2, bT$) facilitates the possibility of realising automated flux control for each qubit. Indeed, if we want to set the fluxes $(f_{q1}^0, f_{q2}^0, f_{q3}^0)$ in the qubits, we should feed the bias lines with the direct currents: $I_{bj}^0 = \Phi_0 \sum_i M_{qi,bj}^{-1} f_{qi}^0$. Fig 3 shows $-\tan \theta(f_{q2}, f_{q3})$ for different fluxes through qubit 1. The left column (a, c, e, g, i) represents the tank circuit phase shift, measured at a base temperature of 10 mK, while the right column (b, d, f, h, j) is the theoretical prediction [18] for the sample parameters determined from the Fig 2. The experimental and theoretical data are in good agreement.

Fig.3 can be understood if one looks at the ground state in the classical limit ($\Delta_1 \rightarrow 0$, $\Delta_2 \rightarrow 0$, $\Delta_3 \rightarrow 0$). In that case we have sharp crossovers between the basis states. In

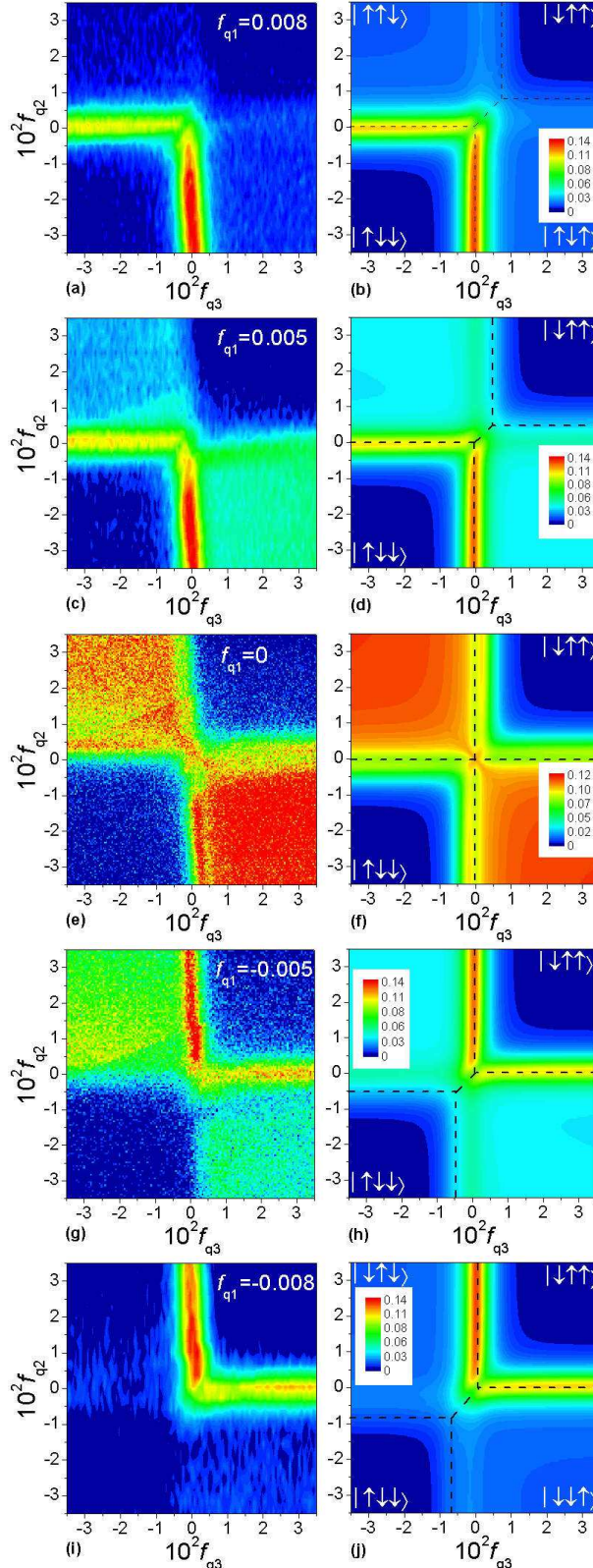


Fig. 3 – Plot of $-\tan \theta(f_{q2}, f_{q3})$ for different fluxes f_{q1} through qubit 1. The left column (a, c, e, g, i) represents the tank circuit phase shift, measured for a mixing chamber temperature of 10 mK, while the right column (b, d, f, h, j) is the theoretical prediction for a qubit-system at $T_{\text{eff}} = 70$ mK. The black dashed lines denote the cross-overs between the different classical states. The imperfect compensation visible in the upper left corner is due to the saturation of one of the current sources, therefore the points there have a slightly larger $|f_{q1}|$.

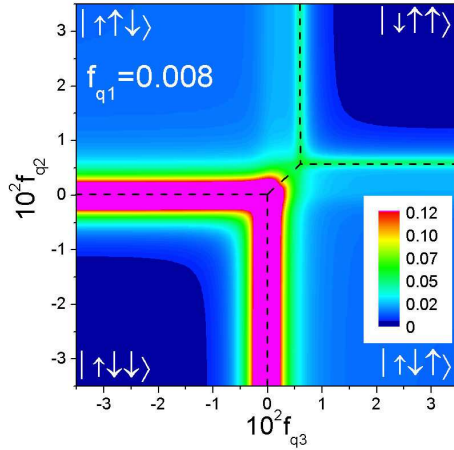


Fig. 4 – $\tan \theta(f_{q2}, f_{q3})$ at $f_{q1} = 0.008$ for hypothetical qubit parameters: $J_{12} = J_{13} = J_{23} = 0.3$ K, $I_{p1} = 130$ nA, $I_{p2} = I_{p3} = 180$ nA, $T_{\text{eff}} = 70$ mK. All other parameters are the same as in experiment. Dashed lines denote the classical cross-overs between the different two-qubit states, signal above 0.12 is marked by magenta colour.

the figures they are indicated by black dashed lines between the states $|\uparrow_1\uparrow_2\downarrow_3\rangle$, $|\downarrow\uparrow\uparrow\rangle$, $|\uparrow\downarrow\downarrow\rangle$ and $|\uparrow\downarrow\uparrow\rangle$ in Fig 3b and the states $|\downarrow\uparrow\downarrow\rangle$, $|\downarrow\uparrow\uparrow\rangle$, $|\uparrow\downarrow\downarrow\rangle$ and $|\downarrow\downarrow\uparrow\rangle$ in Fig 3j. Here the spin-up and spin-down notation describes different directions of the persistent current in the qubit loops. There is also a crossover from $|\uparrow\uparrow\downarrow\rangle$ and $|\uparrow\downarrow\uparrow\rangle$ to $|\downarrow\uparrow\downarrow\rangle$ and $|\downarrow\downarrow\uparrow\rangle$ at the plane of Fig 3f ($f_{q1} = 0$). The ferromagnetic states $|\uparrow\uparrow\uparrow\rangle$ and $|\downarrow\downarrow\downarrow\rangle$ are not reached for this flux subspace, because of their relatively high energies.

For finite Δ_i macroscopic quantum tunnelling removes the classical degeneracy and the qubit's wave function becomes a superposition of the spin states in the vicinity of the anti-crossing. As a result the ground and first excited state of the multi-qubit system exhibit significant curvature. In accordance with formula (1) the phase shift is maximal at the anti-crossings and from the measurements one would be able to reconstruct the classical anti-crossing curves. Nevertheless, it is not the case for all parameter space because we measure the susceptibility with respect to the total flux. For the transitions from $|\downarrow\uparrow\uparrow\rangle$ to $|\uparrow\uparrow\downarrow\rangle$ or $|\uparrow\downarrow\uparrow\rangle$ the total “magnetization” does not change, thus there is no susceptibility change and no phase shift. Moreover, for our set of parameters, in the vicinity of these transitions the difference between the ground and first excited state is smaller than the system's effective temperature. Therefore the *ac*-susceptibility is suppressed because of the partial occupation the first excited state [15]. Nevertheless, the transitions would be visible if the persistent currents were different as shown in fig 4. In this case the magnetization of the states mentioned above would be slightly different resulting in a change of the susceptibility at their crossover.

The very good agreement between the measured susceptibility and its prediction underlines the usefulness of the parametric transducer for characterising qubits in the ground state. By using this equilibrium measurement technique we can find some of the anti-crossings for the flux space $|f_{q1}| \gtrsim 0.003$ and all for $|f_{q1}| \lesssim 0.003$. In principle, the range where complete characterization is possible can be increased by either decreasing the effective temperature of the setup, or by fabricating another sample with a higher Δ/J and qubits with different critical currents. As an illustration we calculated the system response (see fig 4) for hypothetical parameters $J = 0.3$ K, $I_{p1} = 130$ nA, $I_{p2} = I_{p3} = 180$ nA and with all the others the same as

for the current sample. Here all classical crossovers are clearly visible even for $T_{\text{eff}} = 70$ mK. By using non-equilibrium measurements with adiabatic evolution it should be possible to determine the state completely. In this kind of measurement one would prepare the system in the ground state at a point where this state is easily reached and, subsequently, let it evolve to the problem Hamiltonian adiabatically slowly but fast enough to avoid thermal excitation.

In conclusion, the three flux qubit susceptibility was completely reconstructed. The experimental data are found to be in complete agreement with quantum mechanical predictions in full parameter space. We also demonstrate a *controllable* multi-qubit ground band anti-crossing read-out, which allows ground-state computation with superconducting flux qubits. The next steps in this direction would be the improvement of the read-out speed and demonstration of adiabatic quantum computation and its efficiency.

A. I., S. v. d. P., E. I. were supported by the EU through the RSFQubit and EuroSQIP projects and M. G. by Grants VEGA 1/2011/05 and APVT-51-016604. We thank E. Goldobin, R. Gross, H. E. Hoenig, S. Linzen, M. J. Storcz, Th. Wagner, and A. Zeilinger for fruitfull discussions.

REFERENCES

- [1] MAKHLIN YU., SCHÖN G. and SHNIRMAN A., *Rev. Mod. Phys.*, **73** (2001) 357; WENDIN G., SHUMEIKO V. S., cond-mat/0508729; YOU J. Q., NORI FRANCO, *Phys. Today*, **58** (2005) 42.
- [2] PASHKIN YU. A. *et al.*, *Nature*, **421** (2003) 823.
- [3] YAMAMOTO T. *et al.*, *Nature*, **425** (2003) 941.
- [4] McDERMOTT R. *et al.*, *Science*, **307** (2005) 1299.
- [5] CHIORESCU I. *et al.*, *Nature*, **431** (2004) 159.
- [6] WALLRAFF A. *et al.*, *Nature*, **431** (2004) 162.
- [7] MARTINIS J. M. *et al.*, *Phys. Rev. Lett.*, **95** (2005) 210503; LUPAȘCU A. *et al.*, *Phys. Rev. Lett.*, **96** (2006) 127003; BERTET P. *et al.*, *Phys. Rev. Lett.*, **95** (2005) 257002; ITHIER G. *et al.*, *Phys. Rev. B*, **72** (2005) 134519; SIDDIQI I. *et al.*, *Phys. Rev. B*, **73** (2005) 054510; WALLRAFF A. *et al.*, *Phys. Rev. Lett.*, **95** (2005) 060501; IL'ICHEV E. *et al.*, *Phys. Rev. Lett.*, **91** (2003) 097906;
- [8] FARHI E., GOLDSTONE J., GUTMAN S. and SIPSER M., quant-ph/0001106.
- [9] KAMINSKY W.M., LLOYD, S. and ORLANDO T. P., quant-ph/0403090.
- [10] AHARONOV D. *et al.*, quant-ph/0405098.
- [11] MOOIJ J. E. *et al.*, *Science*, **285** (1999) 1036; ORLANDO T. P. *et al.*, *Phys. Rev. B*, **60** (1999) 15398.
- [12] SILVER A. H. and ZIMMERMAN J. E. , *Phys. Rev.*, **157** (1967) 317.
- [13] IL'ICHEV E. *et al.*, *Appl. Phys. Lett.*, **80** (2002) 4184.
- [14] GRAJCAR M., IZMALKOV A. and IL'ICHEV E., *Phys. Rev. B*, **71** (2005) 144501.
- [15] GRAJCAR M. *et al.*, *Phys. Rev. B*, **72** (2005) 020503(R).
- [16] STEFFEN M. *et al.*, *Phys. Rev. Lett.*, **90** (2003) 067903.
- [17] GRAJCAR M. *et al.*, *Phys. Rev. Lett.*, **96** (2006) 047006.
- [18] IZMALKOV A. *et al.*, *Phys. Rev. Lett.*, **93** (2004) 037003; SMIRNOV A. YU., cond-mat/0312635.
- [19] MAJER J. B. *et al.*, *Phys. Rev. Lett.*, **94** (2005) 090501
- [20] YOU J. Q., NAKAMURA Y., NORI F., *Phys. Rev. B*, **71** (2005) 024532.
- [21] LEVITOV, L. S., ORLANDO T. P., MAJER J. B. and MOOIJ J. E., cond-mat/0108266.
- [22] GREENBERG YA. S. *et al.*, *Phys. Rev. B*, **66** (2002) 214525; GRAJCAR M. *et al.*, *Phys. Rev. B*, **69** (2004) 060501(R).